analytical chemistry

pubs.acs.org/ac Article

Single-Nanoparticle Collision Electrochemistry Biosensor Based on an Electrocatalytic Strategy for Highly Sensitive and Specific Detection of H7N9 Avian Influenza Virus

Yan-Ju Yang, Yi-Yan Bai, Yue-Yue Huangfu, Xiao-Yan Yang, Yi-Shen Tian, and Zhi-Ling Zhang*

Cite This: *Anal. Chem.* 2022, 94, 8392−8398 Read Online

ACCESS | Metrics & More | Article Recommendations | Supporting Information

ABSTRACT: Single-nanoparticle collision electrochemistry (SNCE) has gradually become an attractive analytical method due to its advantages in analytical detection, such as a fast response, low cost, low sample consumption, and in situ real-time detection of analytes. However, the biological analyte's direct detection based on the SNCE blocking mode has the problems of low sensitivity and specificity. In this work, an SNCE biosensor based on SNCE electrocatalytic strategy was used for the detection of H7N9 AIV. Nucleic acid aptamers were introduced to recognize the target virus (H7N9 AIV). After the recognition event, $ssDNA_1$ was released and hybridized with another $ssDNA_2$. Owing to the nicking endonuclease Nt.AlwI-mediated target nucleic acid cyclic amplification, one virus particle can indirectly induce the release of 4.2×10^6 Au NPs that can be counted by the SNCE electrocatalytic strategy. The high conversion efficiency greatly improved the detection sensitivity, and the detection limit was as low as 24.3 fg/mL. Therefore, the constructed biosensor can achieve a highly sensitive and specific detection of H7N9 AIV and show a great potential in bioanalytical application.

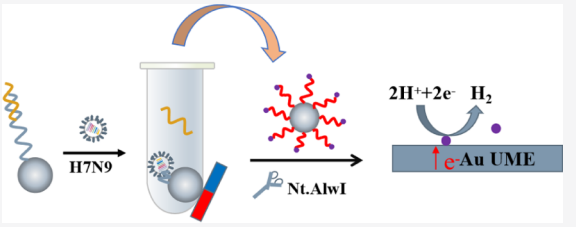

INTRODUCTION

In recent years, single-nanoparticle collision electrochemistry (SNCE) has gradually developed to be an emerging nanoparticle analysis method.[1−4] The main process is that upon applying a specific voltage to the electrode, nanoparticles in the solution are driven by Brownian motion to the microelectrode surface and collide with an electrode, resulting in transient electrochemical signals.[5] According to the different reaction modes of the interaction between nanoparticles and the microelectrode, the typical reactions of a single-nanoparticle collision can be divided into three categories: blocking, electrocatalytic, and particle self-electrolysis.[6] In the blocking mode, insulating nanoparticles collide with a microelectrode or even adhere to the electrode surface and further hinder the original redox reaction of electroactive substances on the electrode, resulting in reduced step-like current transients. The information about nanoparticles can be directly obtained by analyzing the staircase current transients. As for the electrocatalytic mode, electroactive nanoparticles with catalytic properties, such as Pt NPs,[7,8] Au NPs,[9,10] collide with an inert microelectrode, by which electroactive species in the solution are catalyzed. Also, step-like or peak-like signals are generated. Moreover, in the self-electrolysis mode, chemical signals can be observed because of the self-electrolysis of nanoparticles such as Ag NPs.[11,12]

Based on SNCE, information such as the size,[13,14] catalytic performance,[15,16] concentration,[17] and aggregation[18] of a single nanoparticle could be acquired. At the same time, SNCE has the advantages of a fast response, simple operation, low cost, and low sample consumption. Therefore, there is great application potential and value in the detection of biological analytes by SNCE.[19] Since Bard's group first used SNCE to detect DNA in 2012,[20] the method of SNCE has received more attention in the detection of biological analytes and has been used for the detection of DNA,[21] RNA,[22] proteins,[23] viruses,[24] and so forth. Specifically, early studies mainly adopted the SNCE blocking mode to detect biological analytes directly. The current flux was reduced by a collision with the microelectrode of insulating biological analytes. In the SNCE blocking mode, the detection specificity is limited due to electrochemical collision signals, which may be generated by nontarget analytes. At the same time, if the biological analyte adheres to the electrode surface, it may cause contamination of the electrode.[25,26] Compared with the blocking mode, the SNCE electrocatalytic mode has a higher accuracy and specificity. The SNCE electrocatalytic mode can produce more significant current changes, which are beneficial to the statistics and analysis of signals. The accuracy of detection is enhanced. Besides, the application of the electrocatalytic mode

Received: February 24, 2022
Accepted: May 24, 2022
Published: June 3, 2022

https://doi.org/10.1021/acs.analchem.2c00913
Anal. Chem. 2022, 94, 8392−8398

Scheme 1. Schematic Illustration of a Single-Nanoparticle Collision Electrochemistry Biosensor for the Highly Sensitive and Specific Detection of H7N9 AIV[a]

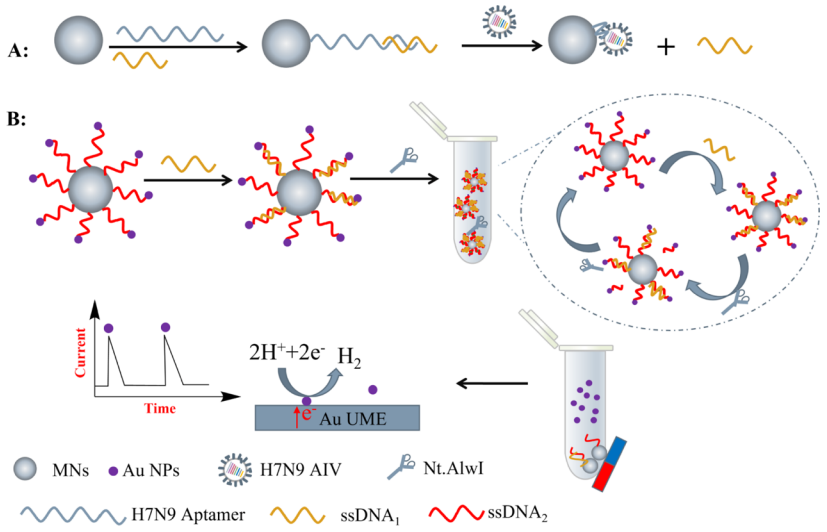

[a](A) Schematic of $ssDNA_1$ releasing. (B) Nicking endonuclease Nt.AlwI-mediated target recycling and Au NP release for the electrochemical single-nanoparticle collision measurement.

mainly relies on the indirect conversion of biological analytes into catalytic nanoparticles.[27,28] In this process, through the introduction of specific recognition of targets, such as antibodies and aptamers, the specificity of the method can be greatly improved. However, in present applications, the SNCE electrocatalysis mode is mainly used for the analysis of the basic properties of nanoparticles.[11,29,30] Recently, a few studies focusing on electrocatalysis and direct electrolysis of nanoparticles for bioanalytical detection have been reported.[8,21−23,31,32] While the SNCE electrocatalytic method for bioanalytical detection has not been systematically developed, the detection sensitivity needs to be further improved. Therefore, it is necessary to develop a biosensor by taking a full advantage of the SNCE electrocatalytic mode and with the help of an efficient signal amplification strategy to achieve a highly sensitive and specific detection of biological analytes.

Here, we proposed an SNCE biosensor (SNCEB) based on the SNCE electrocatalytic mode for a highly sensitive and specific detection of the H7N9 avian influenza virus (AIV). First, nucleic acid aptamers were used for the recognition of the target virus (H7N9 AIV). Single-strand DNA_1 ($ssDNA_1$) was released after the recognition event and hybridized with another single-strand DNA_2 ($ssDNA_2$). After that, with the help of an enzyme Nt.AlwI, Au NPs were released and participated in a single-nanoparticle collision test to quantify the target virus particles. In order to improve the sensitivity and specificity of detection, nucleic acid aptamers were introduced into this work, and the detection of H7N9 AIV was converted to the detection of nucleic acids. Owing to the diverse and flexible amplification strategies of nucleic acids, the method can be widely applicated in biosensing. The specificity of the method was greatly improved based on the specific recognition of H7N9 AIV and its aptamers. Also, magnetic nanospheres (MNs) in this work were used to improve the convenience of separation. At the same time, the use of the nicking endonuclease Nt.AlwI can mediate the cyclic amplification of the target nucleic acid.[33] Also, in the presence of the nicking endonuclease Nt.AlwI, one virus particle can indirectly induce the release of multiple Au NPs that can be counted by the SNCE electrocatalytic strategy. Therefore, the highly sensitive and specific detection of H7N9 AIV was achieved based on the proposed SNCEB.

EXPERIMENTAL SECTION

Single-Nanoparticle Collision Electrochemistry Test. The single-nanoparticle collision electrochemical test was carried out in a Faraday cage, using a three-electrode system, Ag/AgCl (3 M KCl) as the reference electrode, Pt wire as the counter electrode, and Au UME as the working electrode, respectively. The electrolyte was a 0.8 mM $HClO_4$ solution, the voltage was set to −0.4 V, and the data sampling interval was 3 ms for i−t experiments. Before testing, nitrogen was introduced into the electrolyte solution for 30 min to fully eliminate the dissolved oxygen. Then, the sample was added into the solution and stirred with nitrogen bubbles for 1 min.

Preparation of MNs-apt-$ssDNA_1$. MNs were synthesized by the method previously reported,[34] and the preparation of aptamer-modified MNs (MNs-apt) was based on the interaction of biotin and streptavidin (SA). First, 6 mg of *N*-(3-dimethylaminopropyl)-*N*′-ethylcarbodiimide hydrochloride (EDC) and 3 mg of *N*-hydroxysuccinimide (NHS) were added to 1.2 mg/mL of MNs, respectively, in 600 μL of a 0.01 M phosphate buffer solution (PBS, pH = 6.8) to react for half an hour at room temperature. Next, 6 μL of 5 μg/μL SA was added to the above solution for 4 h at 37 °C to obtain streptavidin-modified MNs (MNs-SA). After that, 2 μL of 100 μM biotin-modified aptamer was reacted with 50 μL of prepared MNs-SA for 1 h at 37 °C. Finally, the conjugates were dealt with 0.01 M PBS (pH = 7.2) containing 1% BSA for half an hour and washed 3 times with 0.01 M PBS (pH = 7.2) until the supernatant was free of foam and the MNs-apt was obtained.

The preparation of MNs-apt-$ssDNA_1$ was based on the partial complementary pairing of the aptamer and $ssDNA_1$. 2 μL of 100 μM $ssDNA_1$ and 50 μL of MN-apt were mixed and reacted at 37 °C for 2 h. After washing 5 times, MN-apt-$ssDNA_1$ dispersed in 0.01 M PBS (pH = 7.2) was obtained.

https://doi.org/10.1021/acs.analchem.2c00913
Anal. Chem. 2022, 94, 8392−8398

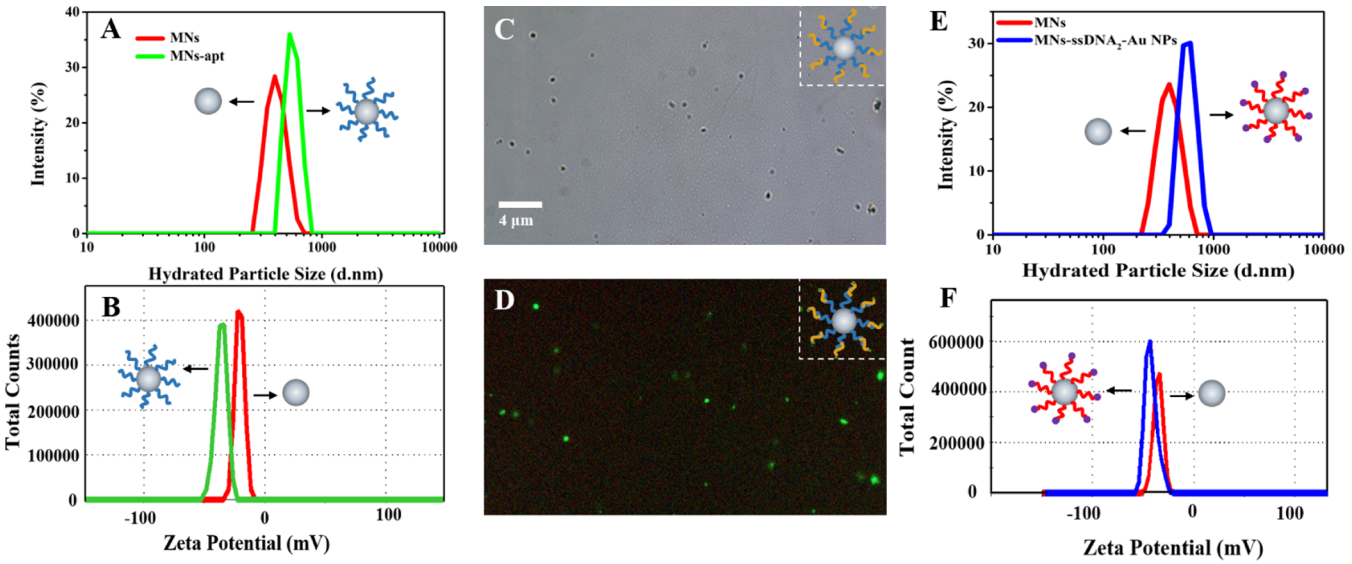

Figure 1. Change of the hydrated particle size (A) and ζ potential (B) of MNs after modification of the aptamer. Bright-field image (C) and fluorescence-field image (D) of MNs-apt-ssDNA$_1$. Change of the hydrated particle size (E) and ζ potential (F) of MNs after modification of ssDNA$_2$ and Au NPs.

Preparation of MNs-ssDNA$_2$-Au NPs. MNs-ssDNA$_2$-Au NPs were prepared according to published work with slight changes.[35] Specifically, 6 μL of 100 μM ssDNA$_2$, 12 μL of 4 mM tris(2-carboxyethyl) phosphine (TCEP), and 12 μL of 0.01 M PBS (pH = 7.2) were mixed and reacted at 37 °C for 1 h. The ssDNA$_2$ solution was then added to 300 μL of MNs-SA, and the rest of the operation was similar to the preparation method of MNs-apt mentioned above. Briefly, SA-modified MNs interacted with biotin-modified ssDNA$_2$ to obtain MNs-ssDNA$_2$ conjugates.

After that, 500 μL of 6 nM Au NPs was incubated with 50 μL of MNs-ssDNA$_2$ overnight at 4 °C. Then, 10 μL of 1% SDS was added to the above solution with gentle shaking at 25 °C for 1 h. Then, 40 μL of 1 M NaCl was slowly added to the mixture and incubated for 12 h. Finally, the mixture was washed 3 times with 0.01 M PBS (pH = 7.2) containing 0.01% SDS until the supernatant was colorless, and the MNs-ssDNA$_2$-Au NPs were obtained.

Quantitative Detection of H7N9. 50 μL of H7N9 AIV with different concentrations was added to MNs-apt-ssDNA$_1$ with gentle shaking at 37 °C for 3 h. After that, the released ssDNA$_1$ solution was added and reacted with MNs-ssDNA$_2$-Au NPs for 1 h at 37 °C. Then, a commercial magnetic scaffold was used to carefully remove the supernatant, and then 10 μL of 0.01% SDS, 5 μL of 10 × NEB buffer, 1 μL of Nt.AlwI, and 34 μL of sterilized water were added to the MNs-ssDNA$_2$-Au NPs at 37 °C for 1.5 h. The supernatant Au NPs were separated, and 20 μL of supernatant was added to 20 mL 0.8 mM $HClO_4$ for single-nanoparticle collision electrochemical tests.

RESULTS AND DISCUSSION

Detection Principle of the SNCEB. The detection principle of the SNCEB was illustrated in Scheme 1. Specifically, the H7N9 AIV aptamers were immobilized on the surface of MNs and partially hybridized with ssDNA$_1$ to form H7N9-apt-ssDNA$_1$ conjugates. H7N9 AIV was recognized by the aptamers specifically, and the H7N9-apt-ssDNA$_1$ conjugates released ssDNA$_1$ into the supernatant. The released ssDNA$_1$ was then hybridized with ssDNA$_2$, which was linked with Au NPs and bound to MNs (MNs-ssDNA$_2$-Au NPs) to form the double-stranded DNA. In the presence of the nicking endonuclease Nt.AlwI, the ssDNA$_2$ in the double-stranded DNA containing the specific recognition sequence of -GGATC- was cleaved while ssDNA$_1$ remained unchanged. Also, ssDNA$_1$ was released to participate in the next round of recycling to achieve the purpose of cyclic amplification. At the same time, the Au NPs attached to ssDNA$_2$ were cleaved and used for electrochemical detection. The released Au NPs collided effectively with the Au ultramicroelectrode (Au UME) in a perchloric acid electrolyte under a specific voltage. By counting the SNCE frequencies of Au NPs, the concentration of H7N9 AIV can be obtained indirectly. Therefore, the SNCEB based on the electrocatalytic mode for the highly sensitive and specific detection of H7N9 AIV was constructed.

Preparation and Characterization of MNs-Apt-ssDNA$_1$ and MNs-ssDNA$_2$-Au NPs. For the successful construction of the SNCEB, MNs-apt-ssDNA$_1$ and MNs-ssDNA$_2$-Au NPs conjugates were prepared, respectively. MNs were used in the SNCEB because of their excellent separation and enrichment capabilities. The average hydrated particle size of the synthesized MNs was about 415.2 nm (Supporting Information Figure S1B), and MNs can be almost completely enriched within 180 s by a commercial magnetic scaffold (Supporting Information Figure S1C), which indicated a good magnetic response of the synthesized MNs. Next, the biotinylated aptamer was coupled to the surface of MNs-SA. Dynamic light scattering (DLS) was used to characterize the hydrated particle size and ζ potential of MNs before and after coupling the aptamer. After coupling the aptamer, the hydrated particle size increased from 410.9 to 566.3 nm (Figure 1A), and the ζ potential changed from −20.9 to −36.1 mV (Figure 1B), indicating the successful preparation of MNs-apt. Then, to confirm the successful preparation of MNs-apt-ssDNA$_1$, FAM fluorescently labeled ssDNA$_1$ was hybridized with MNs-apt. From the images of the bright field (Figure 1C) and fluorescence field (Figure 1D), it can be observed that there was an obvious fluorescence after hybridization with ssDNA$_1$,

https://doi.org/10.1021/acs.analchem.2c00913
Anal. Chem. 2022, 94, 8392−8398

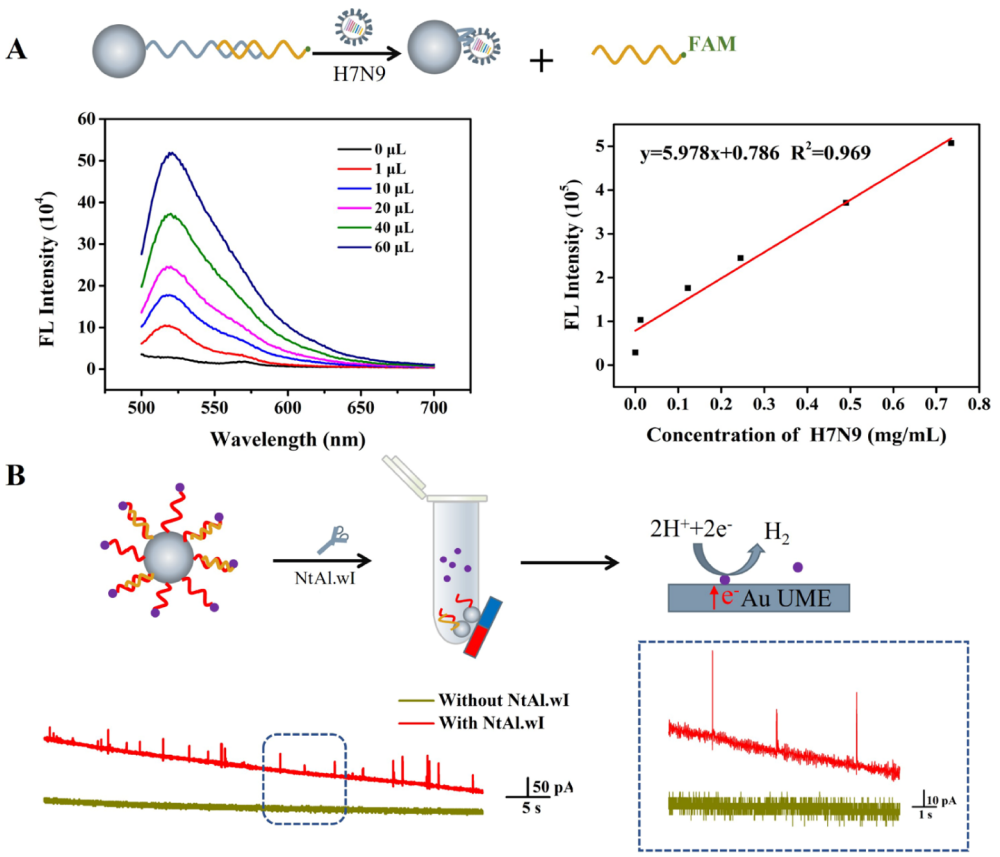

Figure 2. (A) Relationship between released the ssDNA$_1$-FAM fluorescence intensity and the concentration of H7N9 AIV. (B) Chronoamperometric i−t curve without (green) and with (red) the nicking endonuclease Nt.AlwI. The dashed box is a partially enlarged view of the current transients.

and MNs-apt-ssDNA$_1$ conjugates were constructed successfully.

MNs-ssDNA$_2$-Au NPs conjugates were prepared based on the traditional salt aging method. Au nanoparticles (Au NPs) were synthesized by the sodium citrate method.[36] Also, the size distribution histogram and UV−vis absorption spectroscopy of synthetic Au NPs were reported in the Supporting Information Figure S2. Au NPs were connected to MN-ssDNA$_2$ based on a gold−thiol bond interaction. Specifically, the preparation method of MNs-ssDNA$_2$ was similar to that of MNs-ssDNA$_1$. Moreover, the concentration of added ssDNA$_2$ was optimized to 2 μM (Supporting Information Figure S3). Besides, the preparation process of MNs-ssDNA$_2$-Au NPs was also optimized. As shown in the Supporting Information Figure S4, MNs-ssDNA$_2$-Au NPs presented a transparent wine-red color and kept stable when both TCEP and 1% BSA were used; otherwise, the mixture was in an aggregation state and presented a dark color, just like the phenomenon in the absence of ssDNA$_2$. In this process, TCEP was used to reduce the disulfide bonds that formed during the operation and storage of the thiol-modified ssDNA$_2$ so that Au NPs can react with ssDNA$_2$ as fully as possible. Besides, 1% BSA was added to MNs-ssDNA$_2$ to avoid the nonspecific adsorption of Au NPs on the surface of MNs. DLS was used to characterize MNs-ssDNA$_2$-Au NPs. The hydrated particle size increased from 402.7 to 588.3 nm (Figure 1E) after Au NPs coupling. Also, since the surface of Au NPs was negatively charged, the ζ potential shifted negatively from −34.9 to −42.3 mV (Figure 1F) after Au NPs coupling. All the pieces of evidence indicated that the MNs-ssDNA$_2$-Au NP conjugates were successfully constructed.

Feasibility of the Single-Nanoparticle Collision Electrochemistry Biosensor. To illustrate the feasibility of the SNCEB, the feasibilities of H7N9 AIV addition to release ssDNA$_1$ from MNs-apt-ssDNA$_1$ and enzymatic cleavage to obtain Au NPs were verified separately. First, it was necessary to verify whether the ssDNA$_1$ can be released successfully. The ssDNA$_1$ was labeled with the FAM fluorescent dye to prepare MNs-apt-ssDNA$_1$-FAM, and different concentrations of H7N9 AIV were added to react with MNs-apt-ssDNA$_1$-FAM. After the reaction, the supernatant containing ssDNA$_1$-FAM was magnetically separated, and the intensity of the ssDNA$_1$-FAM supernatant was measured using a fluorescence spectrophotometer. As shown in Figure 2A, with an increasing H7N9 AIV concentration, the fluorescence intensity of ssDNA$_1$-FAM obtained from the supernatant also increased. It means that H7N9 AIV can successfully replace ssDNA$_1$ from MNs-apt-ssDNA$_1$.

Next, the feasibility of the enzymatic cleavage to obtain Au NPs was further explored. Au NPs obtained from the experimental group (with Nt.AlwI) and the control group (without Nt.AlwI) were respectively subjected to electrochemical tests. In the electrochemical tests, the voltage was set to −0.4 V (Supporting Information Figure S5), and Au UME (Supporting Information Figure S6) with a radius of 38 μm was used as the working electrode. Au UME was prepared by flame sintering and the sealing method.[37] The chronoamperometric i−t curve without (green) and with (red) the nicking

https://doi.org/10.1021/acs.analchem.2c00913
Anal. Chem. 2022, 94, 8392−8398

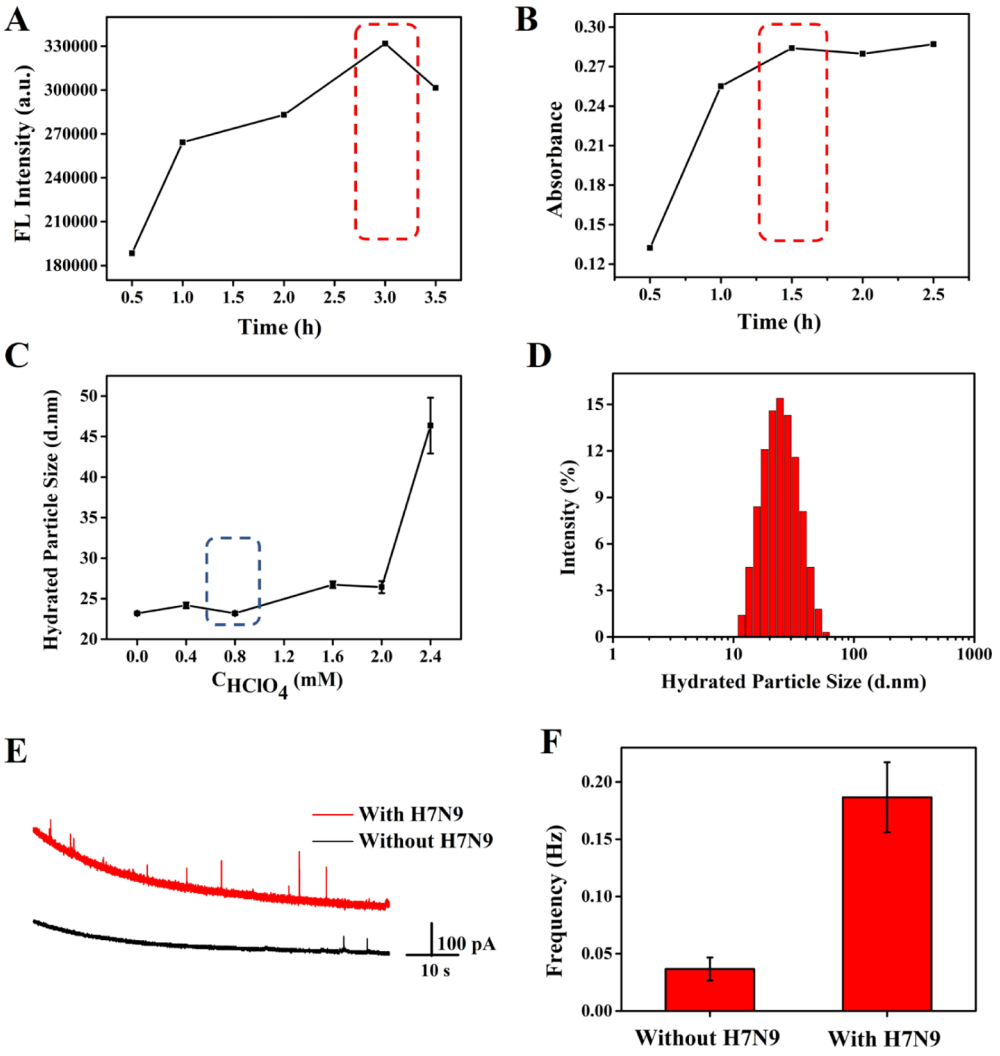

Figure 3. Optimization of the reaction time of ssDNA$_1$ release (A) and enzyme cleavage reaction time (B). (C) Hydrated particle size of Au NPs in different concentrations of perchloric acid. (D) Hydrated particle size histogram of Au NPs in 0.8 mM perchloric acid. (E) Chronoamperometric i−t curve without (black) and with (red) 2 pg/mL H7N9 AIV. (F) Comparison of the collision frequency without and with 2 pg/mL H7N9 AIV.

endonuclease Nt.AlwI was shown in Figure 2B. When there was no nicking endonuclease Nt.AlwI, the Au NPs cannot be cleaved, and no collision signal was found. Conversely, in the presence of Nt.AlwI, the Au NPs were released due to a specific enzyme cleavage, and collision events were produced. All the above results confirmed that the proposed SNCEB could work effectively.

Optimization of Detection Conditions and Feasibility of the Highly Sensitive Detection of H7N9 AIV. The reaction time of ssDNA$_1$ release (Figure 3A) and the enzyme cleavage reaction time (Figure 3B) were optimized, respectively. Also, the optimal reaction time of ssDNA$_1$ release was 3 h, and the enzyme reaction time was optimized to be 1.5 h. In single-particle collision electrochemical detection, the dispersibility of Au NPs has an influence on the current intensity and collision frequency of SNCE. Therefore, it is necessary to optimize the concentration of perchloric acid to avoid the aggregation of Au NPs. As shown in Figure 3C, the hydrated diameter of Au NPs kept relatively stable in a low concentration of perchloric acid, and when the perchloric acid concentration was increased to 2.4 mM, the hydrated particle size increased sharply. For the purpose of ensuring the monodisperse and stable existence of Au NPs in the perchloric acid during the test, the final concentration of perchloric acid was selected as 0.8 mM. A higher concentration of perchloric acid led to the unstable existence of Au NPs since the negatively charged Au NPs were electrically neutralized in the presence of high concentrations of hydrogen ions, which resulted in the agglomeration of Au NPs and presented a large, hydrated particle size in perchloric acid. Under the 0.8 mM perchloric acid, Au NPs can keep stable, and their average hydrated particle size was about 23.7 nm (Figure 3D). Therefore, SNCE can work effectively in this concentration of electrolyte. Besides, the hydrated particle size of Au NPs at different timepoints was also tested to ensure that Au NPs remained stable within the test time range. As shown in the Supporting Information Figure S7, the hydrated particle size of Au NPs hardly changed during 2 h. Since the electrochemical tests in our experiment were generally within 1 h, therefore, the monodispersity of Au NPs can be ensured within the test time scale. At the same time, the theoretical collision frequency of nanoparticles can be estimated by eq 1

$$f_{\text{theoretical}} = 4D_{\text{NP}}C_{\text{NP}}aN_{\text{A}} \quad (1)$$

where $f_{\text{theoretical}}$ is the theoretical collision frequency, and D_{NP}, C_{NP}, a are the diffusion coefficient of NPs, the molar

https://doi.org/10.1021/acs.analchem.2c00913
Anal. Chem. 2022, 94, 8392−8398

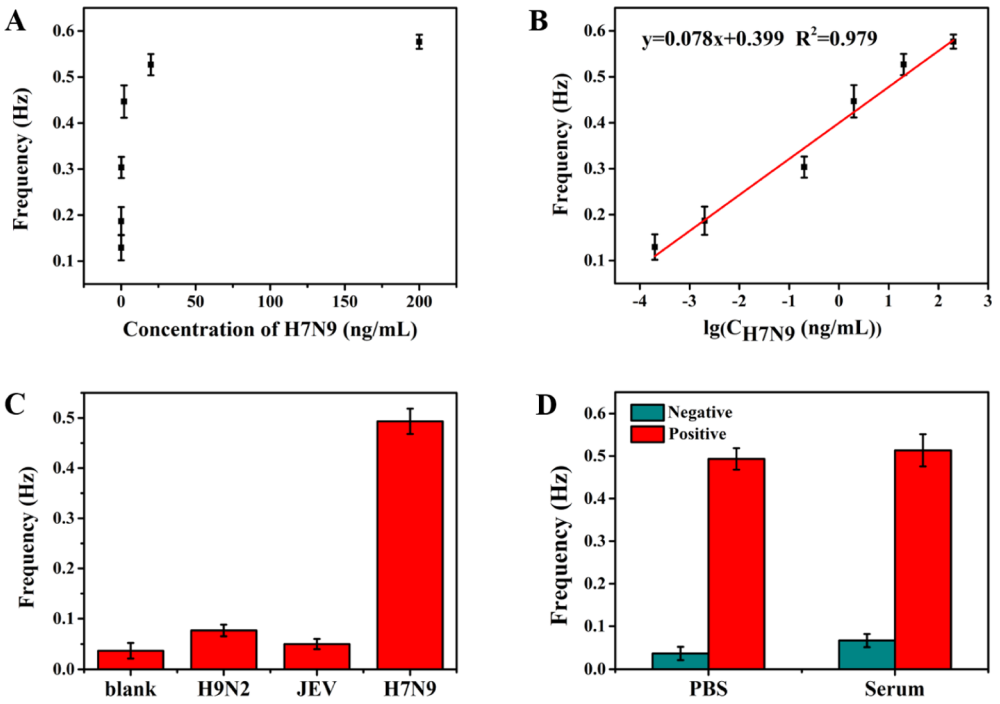

Figure 4. (A) Relationship between the H7N9 AIV concentration and the SNCE frequency. (B) Linear relationship between the logarithmic value of the H7N9 AIV concentration and the single-particle collision electrochemistry frequency. (C) Specificity of the single-nanoparticle collision electrochemical biosensor; the concentration of each kind of virus was 20 ng/mL. (D) Single-particle collision electrochemical biosensor for complex sample detection.

concentration of NPs, and the radius of the electrode, respectively, and N_A is the Avogadro constant.[29] When other conditions are fixed in the experiment, the collision frequency is proportional to the concentration of NPs, and the formula provides a theoretical basis for quantification of nanoparticles.

The chronoamperometric i−t curve without (black) and with (red) 2 pg/mL H7N9 AIV was shown in Figure 3E. When there was no H7N9 AIV, only a few collision signals of Au NPs appeared. However, H7N9 AIV was recognized by MNs-apt-ssDNA$_1$ when 2 pg/mL H7N9 AIV (approximately 3.80×10^4 particles/mL) was added. Also, ssDNA$_1$ was released to participate in the target cycle amplification mediated by the nicking endonuclease Nt.AlwI. At the same time, Au NPs were obtained by enzymatic cleavage and used for electrochemical collision experiments. As shown in Figure 3F, there were obvious signals when H7N9 was added, and the Au NPs collision frequency was 0.187 Hz. Since Au NPs were added to 20 mL of 0.8 mM $HClO_4$ for electrochemical testing, the approximate concentration of Au NPs obtained from the linear curve (Supporting Information Figure S8B) was 0.27 nM, which was approximately 1.61×10^{11} particles/mL. Therefore, one H7N9 AIV can indirectly induce the release of multiple Au NPs, and the conversion efficiency was as high as $1{:}4.2 \times 10^6$ and such a high conversion efficiency indicated that the signal amplification strategy was effective, and the highly sensitive detection of H7N9 AIV can be achieved based on the SNCEB.

Quantitative Detection of H7N9 AIV. The analytical performance of the proposed SNCEB was explored. As shown in Figure 4A,B, in the concentration range of H7N9 AIV 0.2 pg/mL to 200 ng/mL, there was a good linear relationship between the electrochemical collision frequency and the logarithmic value of the H7N9 AIV concentration. Also, the detection limit was 24.3 fg/mL. The proposed method has a high sensitivity and a wide linear range. At the same time, to test the specificity of the method, different kinds of viruses including H7N9 AIV, H9N2 AIV, and Japanese encephalitis virus (JEV) were involved in the testing (Figure 4C). The high collision frequency of Au NPs can only be detected when H7N9 AIV was added. The collision frequency was almost negligible when H9N2 AIV and JEV were added just like that addition of the blank control, indicating a high specificity of the SNCEB for H7N9 AIV detection.

Besides, to verify the application potential of the proposed method in complex samples, the SNCEB was used for the quantification of H7N9 AIV in serum. 20 ng/mL H7N9 was spiked into the serum and PBS buffer for testing, respectively. As shown in Figure 4D, compared to the results in the PBS buffer, there was almost no significant change in the collision frequency when the biosensor was used for the quantification of H7N9 AIV in serum. Therefore, this method has a great application potential in the detection of complex samples. The anti-interference ability and high sensitivity of the SNCEB may be due to the following reasons: (1) a good separation effect can be achieved by using MNs in complex samples, (2) the specificity of the strategy was improved by the introduction of a nucleic acid aptamer with a high-affinity recognition to H7N9 AIV, and (3) through nicking endonuclease Nt.AlwI-mediated cyclic amplification, one virus particle can indirectly induce the release of 4.2×10^6 Au NPs. With such a high conversion efficiency, a highly sensitive detection of H7N9 AIV was achieved.

CONCLUSIONS

In conclusion, a SNCEB based on the electrocatalytic strategy for a highly sensitive and specific detection of H7N9 AIV was proposed. By utilizing the strong affinity between H7N9 AIV and its aptamer, the detection of the virus was converted into

https://doi.org/10.1021/acs.analchem.2c00913
Anal. Chem. 2022, 94, 8392−8398

the detection of nucleic acids. At the same time, by using the nicking endonuclease Nt.AlwI, one H7N9 AIV can indirectly induce the release of multiple Au NPs. Besides, with the help of the SNCE electrocatalytic strategy, a higher sensitivity and precision were achieved than the direct detection by the blocking mode. Therefore, the proposed SNCEB can be promising for a highly sensitive and specific detection of H7N9 AIV, and it could be expected to broaden the application for the detection of biological analytes.

■ ASSOCIATED CONTENT

Supporting Information

The Supporting Information is available free of charge at https://pubs.acs.org/doi/10.1021/acs.analchem.2c00913.

Details about the synthesis and characterization of MNs and Au NPs, optimization of the modified $ssDNA_2$ on each MN, synthetic process optimization of MNs-$ssDNA_2$-Au NPs, optimization of the applied potential for HER, fabrication and characterization of Au UME, stability of Au NPs in 0.8 mM $HClO_4$ at different timepoints, and relationship between the collision frequency and the Au NP concentration (PDF)

■ AUTHOR INFORMATION

Corresponding Author

Zhi-Ling Zhang − *College of Chemistry and Molecular Sciences, Wuhan University, Wuhan 430072, P. R. China;* orcid.org/0000-0001-7807-2264; Phone: 0086-27-68756759; Email: zlzhang@whu.edu.cn; Fax: 0086-27-68754067

Authors

Yan-Ju Yang − *College of Chemistry and Molecular Sciences, Wuhan University, Wuhan 430072, P. R. China*

Yi-Yan Bai − *College of Chemistry and Molecular Sciences, Wuhan University, Wuhan 430072, P. R. China*

Yue-Yue Huangfu − *College of Chemistry and Molecular Sciences, Wuhan University, Wuhan 430072, P. R. China*

Xiao-Yan Yang − *College of Chemistry and Molecular Sciences, Wuhan University, Wuhan 430072, P. R. China*

Yi-Shen Tian − *College of Chemistry and Molecular Sciences, Wuhan University, Wuhan 430072, P. R. China*

Complete contact information is available at: https://pubs.acs.org/10.1021/acs.analchem.2c00913

Notes

The authors declare no competing financial interest.

■ ACKNOWLEDGMENTS

This work was supported by the National Natural Science Foundation of China (21775111, 22074107).

■ REFERENCES

(1) Quinn, B. M.; van't Hof, P. G.; Lemay, S. G. *J. Am. Chem. Soc.* **2004**, *126*, 8360−8361.

(2) Dasari, R.; Robinson, D. A.; Stevenson, K. J. *J. Am. Chem. Soc.* **2013**, *135*, 570−573.

(3) Kong, N.; Guo, J.; Chang, S.; Pan, J.; Wang, J.; Zhou, J.; Liu, J.; Zhou, H.; Pfeffer, F. M.; Liu, J.; Barrow, C. J.; He, J.; Yang, W. *J. Am. Chem. Soc.* **2021**, *143*, 9781−9790.

(4) Zhang, W.; Li, J.; Xia, X.-H.; Zhou, Y.-G. *Angew. Chem., Int. Ed.* **2022**, *61*, No. e202115819.

(5) Xu, W.; Zou, G. Q.; Hou, H. S.; Ji, X. *Small* **2019**, *15*, 1804908.

(6) Peng, Y.-Y.; Qian, R.-C.; Hafez, M. E.; Long, Y.-T. *Chemelectrochem* **2017**, *4*, 977−985.

(7) Xiao, X.; Fan, F.-R. F.; Zhou, J.; Bard, A. J. *J. Am. Chem. Soc.* **2008**, *130*, 16669−16677.

(8) Bai, Y.-Y.; Wu, Z.; Xu, C.-M.; Zhang, L.; Feng, J.; Pang, D.-W.; Zhang, Z.-L. *Anal. Chem.* **2020**, *92*, 853−858.

(9) Li, Y.; Cox, J. T.; Zhang, B. *J. Am. Chem. Soc.* **2010**, *132*, 3047−3054.

(10) Bai, Y.-Y.; Feng, Z.-T.; Yang, Y.-J.; Yang, X.-Y.; Zhang, Z.-L. *Anal. Chem.* **2022**, *94*, 1302−1307.

(11) Oja, S. M.; Robinson, D. A.; Vitti, N. J.; Edwards, M. A.; Liu, Y.; White, H. S.; Zhang, B. *J. Am. Chem. Soc.* **2017**, *139*, 708−718.

(12) Defnet, P. A.; Zhang, B. *J. Am. Chem. Soc.* **2021**, *143*, 16154−16162.

(13) Zhou, Y.-G.; Rees, N. V.; Compton, R. G. *Angew. Chem., Int. Ed.* **2011**, *50*, 4219−4221.

(14) Cheng, W.; Zhou, X.-F.; Compton, R. G. *Angew. Chem., Int. Ed.* **2013**, *52*, 12980−12982.

(15) Chen, L.; Tanner, E. E. L.; Lin, C.; Compton, R. G. *Chem. Sci.* **2018**, *9*, 152−159.

(16) Zhao, L.-J.; Qian, R.-C.; Ma, W.; Tian, H.; Long, Y.-T. *Anal. Chem.* **2016**, *88*, 8375−8379.

(17) Dick, J. E.; Bard, A. J. *J. Am. Chem. Soc.* **2015**, *137*, 13752−13755.

(18) Sokolov, S. V.; Tschulik, K.; Batchelor-McAuley, C.; Jurkschat, K.; Compton, R. G. *Anal. Chem.* **2015**, *87*, 10033−10039.

(19) Zhang, J.-H.; Zhou, Y.-G. *TrAC, Trends Anal. Chem.* **2020**, *123*, 115768.

(20) Kwon, S. J.; Bard, A. J. *J. Am. Chem. Soc.* **2012**, *134*, 10777−10779.

(21) Luo, F.; Chen, F.; Xiong, Y.; Wu, Z.; Zhang, X.; Wen, W.; Wang, S. *Anal. Chem.* **2021**, *93*, 4506−4512.

(22) Castañeda, A. D.; Brenes, N. J.; Kondajji, A.; Crooks, R. M. *J. Am. Chem. Soc.* **2017**, *139*, 7657−7664.

(23) Zhang, J.-H.; Shen, Q.; Zhou, Y.-G. *ACS Sens.* **2021**, *6*, 2320−2329.

(24) Dick, J. E.; Hilterbrand, A. T.; Strawsine, L. M.; Upton, J. W.; Bard, A. J. *Proc. Natl. Acad. Sci. U.S.A.* **2016**, *113*, 6403−6408.

(25) Dick, J. E.; Renault, C.; Bard, A. J. *J. Am. Chem. Soc.* **2015**, *137*, 8376−8379.

(26) Dick, J. E.; Hilterbrand, A. T.; Boika, A.; Upton, J. W.; Bard, A. J. *Proc. Natl. Acad. Sci. U.S.A.* **2015**, *112*, 5303−5308.

(27) Zhang, Y.; Mao, J.; Ji, W.; Feng, T.; Fu, Z.; Zhang, M.; Mao, L. *Anal. Chem.* **2019**, *91*, 5654−5659.

(28) Sepunaru, L.; Plowman, B. J.; Sokolov, S. V.; Young, N. P.; Compton, R. G. *Chem. Sci.* **2016**, *7*, 3892−3899.

(29) Xiang, Z.-p.; Deng, H.-q.; Peljo, P.; Fu, Z.-y.; Wang, S.-l.; Mandler, D.; Sun, G.-q.; Liang, Z.-x. *Angew. Chem., Int. Ed.* **2018**, *57*, 3464−3468.

(30) Lu, S.-M.; Chen, J.-F.; Peng, Y.-Y.; Ma, W.; Ma, H.; Wang, H.-F.; Hu, P.; Long, Y.-T. *J. Am. Chem. Soc.* **2021**, *143*, 12428−12432.

(31) Karimi, A.; Hayat, A.; Andreescu, S. *Biosens. Bioelectron.* **2017**, *87*, 501−507.

(32) Liu, J.; Ma, C.; Shi, S.; Liu, H.; Wen, W.; Zhang, X.; Wu, Z.; Wang, S. *Biosens. Bioelectron.* **2022**, *207*, 114182.

(33) Zhao, R.-N.; Jia, L.-P.; Feng, Z.; Ma, R.-N.; Zhang, W.; Shang, L.; Xue, Q.-W.; Wang, H.-S. *Biosens. Bioelectron.* **2019**, *144*, 111669.

(34) Wen, C. Y.; Xie, H. Y.; Zhang, Z. L.; Wu, L. L.; Hu, J.; Tang, M.; Wu, M.; Pang, D. W. *Nanoscale* **2016**, *8*, 12406−12429.

(35) Valentini, P.; Fiammengo, R.; Sabella, S.; Gariboldi, M.; Maiorano, G.; Cingolani, R.; Pompa, P. P. *ACS Nano* **2013**, *7*, 5530−5538.

(36) Wu, Z.; Guo, W.-J.; Bai, Y.-Y.; Zhang, L.; Hu, J.; Pang, D.-W.; Zhang, Z.-L. *Anal. Chem.* **2018**, *90*, 1683−1690.

(37) Zhang, Y.; Xu, S.; Qian, Y.; Yang, X.; Li, Y. *RSC Adv.* **2015**, *5*, 77248−77254.